Content-Based Filtering for Fast 3D Reconstruction from Unstructured Web-Based Image Data

Konstantinos Makantasis[1], Anastasios Doulamis[2], Nikolaos Doulamis[2], Marinos Ioannides[3], and Nikolaos Matsatsinis[1]

[1] Technical University of Crete,Chania, Crete, 73100 Greece
[2] National Technical University of Athens,Heroon Polytechniou str. 15773 Athens, Greece
[3] Cyprus University of Technology, Archbishop Kyprianou 30, Lemesos, Cyprus, 3036
konst.makantasis@gmail.com, {adoulam,ndoulam}@cs.ntua.gr,
marinos.ioannides@cut.ac.cy, nikos@ergasya.tuc.gr

Abstract. The huge amount of visual collections provides a unique opportunity for cultural heritage e-documentation and 3D reconstruction. The main difficulty, however, is its unstructured nature. In this paper a new content-based image filtering is proposed to discard image outliers that either confuse or significantly delay the 3D reconstruction process. The presented approach exploits a dense-based unsupervised paradigm applied on multi-dimensional manifolds where images are represented as image points. The multidimensional scaling algorithm is adopted to relate the space of the image distances with the space of Gram matrices to compute the image coordinates. Evaluation on a dataset of about 31,000 cultural heritage images being retrieved from internet collections with many outliers indicate the robustness and cost effectiveness of the proposed method towards an affordable 3D reconstruction.

Keywords: Content-based filtering, image matching, outliers' removal, 3D reconstruction.

1 Introduction

Several billions of images exist nowadays in loosely structured repositories over the web (e.g., Flickr, Picasa) while their number rapidly grows every day. Although such proliferation of billions of photographs, online available for free, provides a unique opportunity for cultural object documentation, there are currently limited technological tools in performing massive 3D object reconstruction.

The main difficulty in exploiting such "wild image collections" for cultural e-documentation is their unstructured nature. Consider, for example, a query on web collections containing the keywords "Acropolis, Parthenon." As response to that query, a large set of image outliers is retrieved, which depict not only the Parthenon monument itself, but also the view of the city of Athens from the Acropolis site. On the other hand, manual annotation is an arduous and inconsistent task, mainly due to the complexity of the visual content, the huge effort required and the subjective human's perception. Therefore, content-based filtering algorithms are necessary for a computationally efficient e-documentation using Web-based images.

M. Ioannides et al. (Eds.): EuroMed 2014, LNCS 8740, pp. 91–101, 2014.

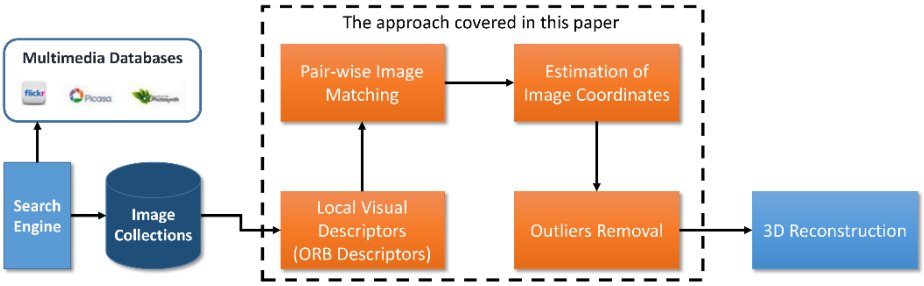

Fig. 1. The pipeline of the proposed methodology.

Content Based Image Retrieval (CBIR) tools that mine images based on visual matching can be considered as content based image filtering and clustering algorithms. The work of [1] proposes a two stage image retrieval process based on color properties. Thus, its performance is inherently depended on camera shutter speed, lens' aperture and scene lighting conditions. Chum et al. in [2] present a system that retrieves all views of an object in a large database exploiting, apart from visual similarities, a vocabulary tree. Similarly, [3] enables user to select regions of interest and then the system returns a ranked list of images using fast spatial matching. The work of [4] proposes the dominant color descriptor to encode visual information, while clustering is performed using fuzzy Support Vectors Machines (fSVMs). Simon et al. in [5] focus on visual clustering implemented through an optimization approach that selects a number of canonical image views for constructing a scene summary. The works of [6] and [7] exploit geo-tagging and annotation to improve the retrieval performance. The idea of geo-clustering is also exploited by the work of [8] for retrieving landmark images. The authors in [9] use geo-tagged datasets from Flickr and assume multiple different views of the same scene/object. The main limitations of these approaches are that they use global image features for visual content organization. This is not, however, suitable for cultural heritage applications and especially for 3D reconstruction purposes where we need to retrieve different views of an object, *laying in the spherical coordinates* that surround this object, instead of using images that they have quite similar content.

In this paper, we propose a fully automatic approach for content-based filtering of Internet stored data used for cultural heritage applications. Filtering is designed in a way to optimize 3D reconstruction engines [10]. Initially, the ORB descriptor [11] (Oriented FAST [12] and Rotated BRIEF [13]) is exploited to visually describe images. Then, a two way pair-wise descriptor matching is applied and similarity matrix is constructed that indicates the distance between every two images. In order to unsupervised remove the image outliers from the retrieved image set, each image is represented as a point onto a multi-dimensional manifold; this is achieved by classical Multi-Dimensional Scaling Algorithm [14] that relates space distance with the space of gram matrices. Manifold image representation has a) a compact hyperspace that contains images depicting different views of the same cultural object and b) spreading samples corresponding to image outliers. Then, the density based spatial clustering

algorithm (DBSCAN) is applied [15] for separating image outliers from the relevant data. Finally, experimental results are presented that indicates the computational improvement achieved by the proposed method in 3D object reconstruction. The pipeline of the proposed methodology is presented in Figure 1.

2 Geometric Invariant Visual Modeling

2.1 ORB-Based Visual Content Representation

In this paper, local visual descriptors, as the ORB descriptor [11], are used to capture the different geometric perspectives of an object. Our choice for a local visual representation is to describe different image views, required for 3D reconstruction, instead of an overall image content description. Additionally, the choice of ORB is justified by the fact that it performs better than SURF [16] and, on the other, it performs as well as SIFT [17], though of two orders of magnitude faster.

ORB descriptor exploits FAST feature detector [12] to locate image keypoints. FAST classifies an image pixel p with intensity of $I(p)$ by extracting a ring of 16 pixels around p and then, compares the intensity values with an appropriate threshold t [11]. Although, FAST does not produce a measure for corners' magnitude, ORB employs a Harris corner measure [18] to order FAST keypoints and pick the top K of them. In this way, ORB reduces the number of extracted corners of FAST to the K most suitable.

2.2 Visual Similarity Degree

For estimating visual similarity between two different images, A and B, their correspondent points have to be computed. Correspondences can be estimated by performing a nearest-neighbor keypoints matching algorithm between every pair of images. Due to the fact that ORB keypoints are described by a binary pattern, multi- probe Locality Sensitive Hashing [19] is used for nearest-neighbor search exploiting the Hamming distance, D_H. Let us denote as $k_i^{(A)}$ the i^{th} keypoint of the image A (extracted via the ORB algorithm) which is described by a feature vector $\mathbf{f}^{(A)}$. Then, the most relevant keypoint $k_{j_i}^{(B)}$ of another image B, described by a feature vector $\mathbf{f}^{(B)}$ with respect to the i^{th} keypoint of image A, $k_i^{(A)}$, is obtained by the following minimization,

$$j_i = \underset{j=1,2,\dots k}{\arg\min}(D_H(\mathrm{f}^{(\boldsymbol{A})}, \mathrm{f}^{(\boldsymbol{B})})) \tag{1}$$

Then keypoints $k_i^{(A)}$ and $k_{j_i}^{(B)}$ are considered as correspondent points. Having detected all correspondent points between two images A and B we can form a set $M^{(A\to B)}$ that contains pairs of all keypoints from the first image A, along with the correspondent points $k_{j_i}^{(B)}$. The set of final matches $M^{(A,B)}$ between images A and B is defined as the intersection of the sets $M^{(A\to B)}$ and $M^{(B\to A)}$. The choice for using a two-way matching is justified by the fact that the nearest neighbor of an extracted

keypoint in image A may be different from the nearest neighbor of the correspondent keypoint in image B. As the number of extracted keypoints for each image is equal to K, we define a visual similarity metric between images $i = A$ and $j = B$ as

$$s_{i=A,j=B} = \frac{\left|M^{(A,B)}\right|}{K} \tag{2}$$

where $\left|M^{(A,B)}\right|$ refers to the cardinality of $M^{(A,B)}$set.

The output of the aforementioned process for Nimages is an $N \times N$ symmetric matrix $\mathbf{S}$ whose elements $s_{i,j} \in [0,1]^T$, with $i, j = 1,2, \ldots N$. Variable $s_{i,j} = 0$ indicates that no relation between the contents of images j and i exists. Instead, for same images $s_{i,j} = 1$. We denote as $\mathbf{D}$ the negative $\log(\mathbf{S})$; similar images receive close to zero while quite dissimilar very high value.

$$\mathrm{D} = \left[\boldsymbol{d_{i,j}}\right] = -\log(\mathrm{S}) \tag{3}$$

$\mathbf{D}$ is a square $N \times N$ symmetric matrix with non-negative elements and zeroes on the main diagonal.

3 Image Representation onto Multidimensional Manifolds

By examining the constructed dissimilarity matrix $\mathbf{D}$, it is easy to be observed that the distance between the visually similar images is small. This means that if images are represented as points onto a multidimensional manifold, then visually similar images will belong to high spatial density subspaces, instead of image outliers which will be spread out onto the space.

Let us define as $\mathbf{x}^{(i)} \in \mathbb{R}^{\mu}$ the coordinates of i^{th} image in the μ-dimensional space. We define the multidimensional space in a way so that the norm (distance) between two points (images) of the space represented by the coordinates $\mathbf{x}^{(i)}$ and $\mathbf{x}^{(j)}$ should be equal to the their respective image distance $d_{i,j} = -\log(s_{i,j})$, i.e., $\left\|\mathbf{x}^{(i)} - \mathbf{x}^{(j)}\right\| = d_{i,j}\ \forall\ i, j$. The coordinates of all N images in the dataset can be compactly represented by a matrix $\mathbf{X} \in \mathbb{R}^{N \times \mu}$.

If we define the Gram matrix $\mathbf{B} = \mathbf{X} \cdot \mathbf{X}^{\mathrm{T}}$ of images' coordinates, then the classical Multi-Dimensional Scaling (cMDS) [14] can be used to establish a connection between the space of the distances and the space of Gram matrix $\mathbf{B}$ based on Theorem 1 [20].

Theorem 1. A non-negative symmetric matrix $\mathbf{D} \in \mathbb{R}^{N \times N}$ with zeroes on the diagonal, is an Euclidean distance matrix if and only if $\mathbf{B} \triangleq -\frac{1}{2}\mathbf{H} \cdot \mathbf{D} \cdot \mathbf{H}$, where $\mathbf{H} \triangleq \mathbf{I} - \frac{1}{N}\mathbf{1} \cdot \mathbf{1}^{\mathrm{T}}$, is positive semidefinite with $\mathbf{I}$ the unit matrix and $\mathbf{1}$ a vector of all ones elements. Furthermore, this $\mathbf{B}$ will be the Gram matrix for a mean centered configuration with interpoint distances given by $\mathbf{D}$ (proof of this theorem can be found in [20]).

In cases where dissimilarity matrix **D** is not Euclidean the matrix **B** as described by the above theorem will not be positive semi-definite, and thus will not be a Gram matrix. To handle such cases, cMDS projects the Gram matrix **B** onto the cone of positive semi-definite matrices by setting its negative eigenvalues to zero. In order to get matrix **X**, the Gram matrix **B** is spectrally decomposed into $\mathbf{U} \cdot \mathbf{V} \cdot \mathbf{U}^{\mathrm{T}}$ and then $\mathbf{X} = \mathbf{U} \cdot \mathbf{V}^{1/2}$. If we denote as q_i and λ_i for $i = 1,2, \ldots, N$ the eigenvectors and eigenvalues of **B**, then matrix **U** is the square $N \times N$ matrix whose i^{th} column is the eigenvector q_i of **B** and **V** is the diagonal matrix whose diagonal elements are the corresponding eigenvalues. Finally the dimension μ of the multidimensional space is equal to the multiplicity of non-zero eigenvalues of matrix **B**.

4 Density Based Partitioning

By representing, the images as points onto the manifold, we are able to remove outliers, improving 3D reconstruction.

4.1 Estimation of Image Spatial Density

The density of an area can be defined as the number of points u existed within a specified radius r on the hyperspace manifold. As no a prior knowledge about the dataset is available, these parameters cannot be set to any predefined value. For this reason, we need a procedure to automatically estimate both r and u parameters.

For a given image A, let us assume that there exists a non-linear relationship, $g^{(A)}(\cdot)$ that relates parameter *u* with the radius *r*. Then $r = g^{(A)}(u)$. Function $g^{(A)}(\cdot)$ indicates the distance required to be defined for a space in order to contain *u* points within radius *r* from image *A*. Function $g^{(A)}(u)$ is monotonically increasing, meaning that as variable *u* increases the radius *r* increases too.

Then, to estimate the best trade-off point between *u* and *r* we adopt the following procedure. First, we define a line segment *l* that connects the points $\mathbf{c}_1 = (u = 1, r = g^{(A)}(1))$ and $\mathbf{c}_N = (u = N, r = g^{(A)}(N))$ onto the *(u,r)* plane. The farthest point of the curve defined by $g^{(A)}(\cdot)$ from the straight line *l* [green line in Figure 2(a)] corresponds to the best trade-off point [21]. To detect this point, initially we define a unit vector as $\mathbf{u} = \mathbf{c}_N - \mathbf{c}_1 / \|\mathbf{c}_N - \mathbf{c}_1\|$. It is clear that vector **u** is parallel to line segment *l*. Then, we define as $\mathbf{v}_i$ a vector that connects points $\mathbf{c}_i = (u = i, r = g^{(A)}(i)$ and $\mathbf{c}_1$. A geometric clarification of the vector $\mathbf{v}_i$ is presented in Figure 2(a). The inner product between vector $\mathbf{v}_i$ and **u**, i.e., $\mathbf{p}_i = \mathbf{u} \cdot \mathbf{v}_i$, projects vector $\mathbf{v}_i$ onto the line segment *l*. Having estimated the vectors $\mathbf{v}_i$ and $\mathbf{p}_i$, we are able to compute a distance between vector $\mathbf{v}_i$ and its projected version onto the line segment *l*.

$$e_i = \|\mathbf{v}_i - \mathbf{p}_i\| \tag{4}$$

Figure **2**(b) plots the distances e_i between curve's points and the straight segment *l* versus *u* parameter for better explanation of the architecture. In the following,

we denote as $e_{\max}^{(A)}$ the maximum value of all e_i, for an image A. It is clear that for another image B a different value of $e_{max}^{(B)}$ is obtained since the non-linear relationship $g^{(B)}(\cdot)$ changes for different images. The procedure is repeated for every image of the dataset and the best image point, say $\hat{\imath}$ is

$$\hat{\imath} = \underset{i=1,2,\ldots,N}{\operatorname{argmax}}(e_{max}^{(i)}) \tag{5}$$

Then, the most appropriate values of r and u, named $\hat{r}$ and $\hat{u}$ respectively are given by the following equation

$$\hat{u} = \underset{i=1,2,\ldots,N}{\operatorname{argmax}}\left(e_{max}^{(i)}\right) \quad \text{and} \quad \hat{r} = g^{\hat{\imath}}(\hat{u}) \tag{6}$$

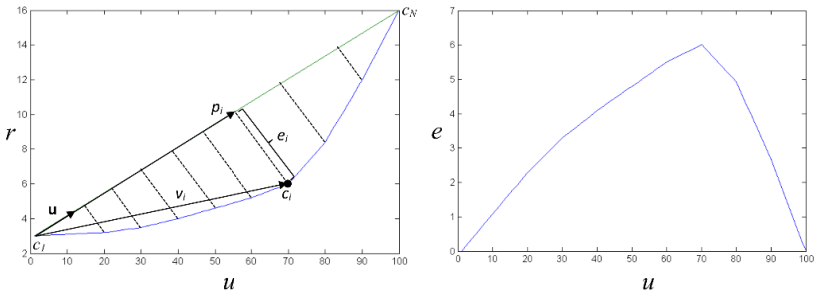

(a) (b)

Fig. 2. Estimation of r variable of DBSCAN in regard to u variable. r can be estimated by the best trade-off point of the curve in blue in diagram (a). For finding the best trade-off point the distance of between every curve's point and the straight line defined by the first and the last points of the curve is computed. The point that presents the biggest distance represents the best trade-off point, diagram in (b).

4.2 Density Based Partitioning

Initially, let us define as $N_r(p)$ a neighborhood of a point $p \in \mathbb{R}^{\mu}$ (image in our case) onto the multidimensional manifold. Neighborhood $N_r(p)$ contains all points $q \in \Theta$, whose distance with respect to p is smaller than or equal to radius r. A point p whose cardinality of neighborhood $|N_r(p)| \geq u$ is called core sample. If a point $q \in N_r(p)$ then points p and q are considered *directly density-reachable*, while two points p and q are considered *density-reachable* if there exists a chain of points $p_1, \ldots, p_n$ with $p_1 = p$ and $p_n = q$ such that p_i is directly density-reachable from p_{i+1}. Finally, two points p and q are considered density connected if there is a core sample o such that both p and q are density-reachable from o with respect to r.

The conventional version of the DBSCAN algorithm creates a compact subset by grouping together all points of the multi-dimensional manifold that are either density

reachable or density connected to a core sample. However, in the context of this paper, we have two types of images. The first type includes the images that potentially contribute to the 3D reconstruction engine (e.g., images of different object views), and the second the outliers. Partitioning the data as the conventional DBSCAN minimizes the probability of excluding relevant images but this also implies that some of the outliers are also included in the target subspace.

An alternative approach, named Core Sample Partitioning (CSP) in this paper, is to set more strict criteria in creating the partitions. In particular, CSP exploits the notion of *directly* density-reachability, i.e. grouping together all points that are *only* directly density reachable to a core sample, creating this way a set that minimizes the probability of an image outlier to belong to the partitioned compact subset. Assuming that a sufficient large set of images depicting a cultural heritage object of interest is available, the proposed modified DBSCAN approach selects images for the 3D reconstruction process that yield low computational complexity, while its precision performance remains almost the same.

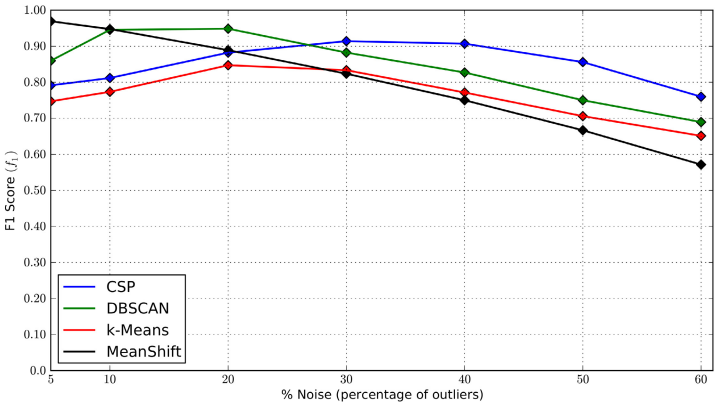

Fig. 3. F1 Score regarding partitioning performance using conventional DBASCAN and the modified CSP along with other clustering approaches

5 Experimental Results

The research presented in this paper is part of 4D-Ch-World project [22]. Using expert's assessment, we have initially annotated a large collection of 31,000 images into two categories; (i) the one of "relevant image set" and (ii) the one of image outliers. For the evaluation, we range the noise, i.e. the ratio of image outliers, in the created datasets from 5% to 60%.

Figure 3 presents the *F*1 Score for two density-based image partitioning approaches that is, of conventional DBSCAN, its modified method called CSP. In Figure 3 we have also compared the center-based clustering of *k*-Means and density-based algorithm of Mean-Shift. The conventional DBSCAN yields better results for small number of outliers (less than 30%) while CSP is more robust for mostly corrupted retrieved data. This is due to the fact that the CSP is more prone to false negatives,

while DBSCAN is more prone to false positives. Both the proposed approaches outperform *k*-Means and Mean-Shift. The precision and recall metrics versus the percentage of noise for the two proposed outliers' removal methods are shown in Figure 4. We observe that precision as regards the CSP approach is higher than the conventional DBSCAN while the opposite is valid as regards the recall metric.

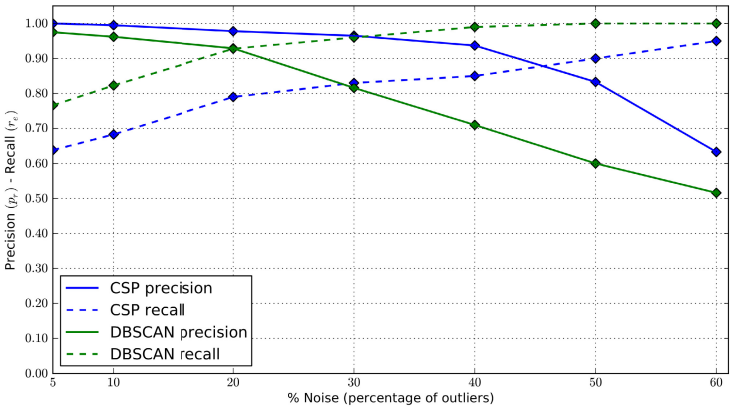

Fig. 4. Precision and recall diagrams for the two different proposed approaches used for outliers removal

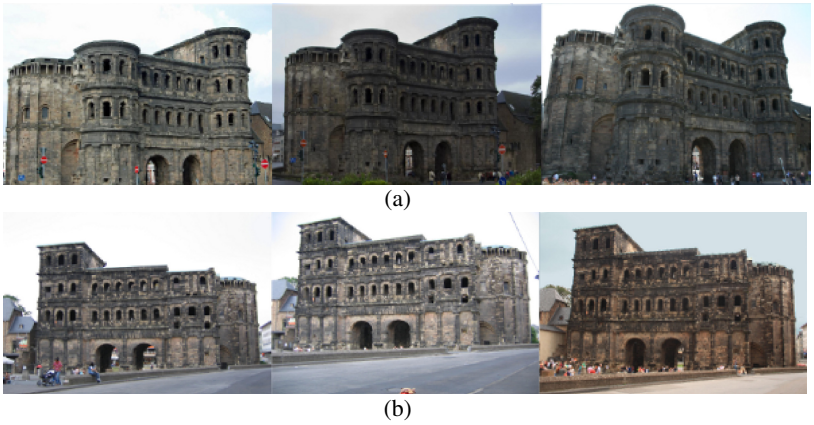

(a)

(b)

Fig. 5. Clustering results for Porta Nigra monument. The first subset (a) includes images that depict the rear side of the monument, while the second subset (b) the front side.

Figure 5 visually depict the clustering results for the Porta Nigra monument. Two partitions are created. Figure 5(a,b) shows characteristic images per partition, where different geometric views are depicted. Finally, Figure 6 presents a 3D reconstruction for the Porta Nigra monument. For this reconstruction we have removed more that 30% of outliers improving reconstruction's computational complexity.

Table 1 presents a quantitative analysis of the performance of the proposed workflow in terms of precision and recall, percentage of reduction of the initial dataset, reconstruction accuracy and computational time. We assume that reconstruction accuracy is 100% when all visually similar images of the initial dataset are used. Furthermore, we denote as *T* the time required for 3D reconstruction when all images of the initial dataset are used. When the total reduction of the initial dataset is large the computational time for 3D reconstruction is very low. For reduction of 30% the reconstruction process can be almost 5 times faster. Figure 6 presents two 3D reconstructed modes of Porta Nigra. These models may seem coarse due to the fact that we used in total only 21 relevant images out of 30 (9 images were denoted as outliers).

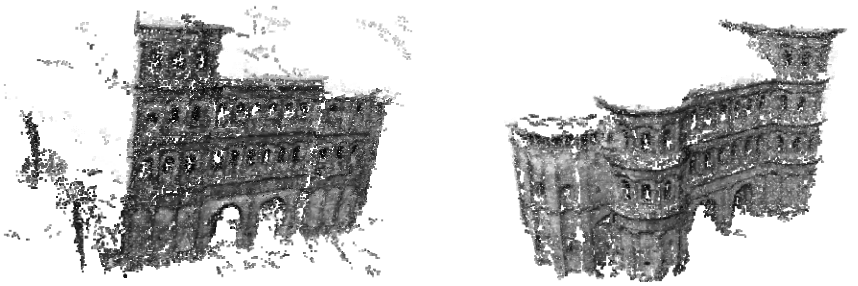

(a) (b)

Fig. 6. 3D reconstruction of Porta Nigra

Table 1. Reconstruction accuracy and computational time

Noise %	Reduction		Precision		Recall		Reconstruction accuracy		Computational cost	
	DB	CSP	DB	CSP	DB	CSP	DB	CSP	DB	CSP
20%	22%	31%	0.94	0.97	0.96	0.81	96%	81%	0.37T	0.22T
30%	30%	28%	0.82	0.96	0.96	0.83	96%	83%	0.24T	0.27T

6 Conclusions

In this paper, we proposed a new content based filtering algorithm that improves the performance and computational efficiency of 3D reconstruction engines. The scheme is robust to highly corrupted retrieved image sets, such as the ones extracted from in the wild image selection. The method represents each image as a point on a multidimensional manifold and methods that relate the coordinates of that space with image distances are exploited. Finally, a modification of the dense based partitioning is introduced. The method is able to select the most appropriate images for 3D reconstruction, improving both performance and computational complexity.

Acknowledgement. The research leading to these results has been supported by Marie Curie IAPP project 4D-CH-World. Grant agreement number 324523.

References

[1] Murthy, V.S., Kumar, S., Rao, P.S.: Content Based Image Retrieval using Hierarchical and K-Means Clustering Techniques. Inter. J. Eng. Sci. Technol. 2 (2010)
[2] Chum, O., Philbin, J., Sivic, J., Isard, M., Zisserman, A.: Total Recall: Automatic Query Expansion with a Generative Feature Model for Object Retrieval. In: IEEE 11th ICCV 2007, pp. 1–8 (2007)
[3] Philbin, J., Chum, O., Isard, M., Sivic, J., Zisserman, A.: Object retrieval with large vocabularies and fast spatial matching. In: IEEE CVPR, pp. 1–8 (2007)
[4] Min, R., Cheng, H.D.: Effective Image Retrieval Using Dominant Color Descriptor and Fuzzy Support Vector Machine. Pattern Recogn. 42(1), 147–157 (2009)
[5] Simon, I., Snavely, N., Seitz, S.M.: Scene Summarization for Online Image Collections. In: IEEE ICCV, Los Alamitos, CA, USA, pp. 1–8 (2007)
[6] Arampatzis, A., Zagoris, K., Chatzichristofis, S.A.: Dynamic Two-Stage Image Retrieval from Large Multimodal Databases. In: Clough, P., Foley, C., Gurrin, C., Jones, G.J.F., Kraaij, W., Lee, H., Mudoch, V. (eds.) ECIR 2011. LNCS, vol. 6611, pp. 326–337. Springer, Heidelberg (2011)
[7] Papadopoulos, S., Zigkolis, C., Kompatsiaris, Y., Vakali, A.: Cluster-based Landmark and Event Detection on Tagged Photo Collections. IEEE Multimed. (2010)
[8] Zheng, Y.-T., Zhao, M., Song, Y., Adam, H., Buddemeier, U., Bissacco, A., Brucher, F., Chua, T.-S., Neven, H.: Tour the world: Building a web-scale landmark recognition engine. In: IEEE CVPR, pp. 1085–1092 (2009)
[9] Agarwal, S., Furukawa, Y., Snavely, N., Simon, I., Curless, B., Seitz, S.M., Szeliski, R.: Building Rome in a Day. Commun. ACM 54(10), 105–112 (2011)
[10] Wu, C., Agarwal, S., Curless, B., Seitz, S.M.: Schematic surface reconstruction. In: IEEE CVPR, pp. 1498–1505 (2012)
[11] Rublee, E., Rabaud, V., Konolige, K., Bradski, G.: ORB: An efficient alternative to SIFT or SURF. In: IEEE ICCV, pp. 2564–2571 (2011)
[12] Rosten, E., Drummond, T.W.: Machine Learning for High-Speed Corner Detection. In: Leonardis, A., Bischof, H., Pinz, A. (eds.) ECCV 2006, Part I. LNCS, vol. 3951, pp. 430–443. Springer, Heidelberg (2006)
[13] Calonder, M., Lepetit, V., Strecha, C., Fua, P.: BRIEF: Binary Robust Independent Elementary Features. In: Daniilidis, K., Maragos, P., Paragios, N. (eds.) ECCV 2010, Part IV. LNCS, vol. 6314, pp. 778–792. Springer, Heidelberg (2010)
[14] Cox, T., Cox, M., Cox, T.: Multidimensional Scaling, 2nd edn. Chapman & Hall/CRC (2000)
[15] Ester, M., Kriegel, H., Sander, J., Xu, X.: A density-based algorithm for discovering clusters in large spatial databases with noise, pp. 226–231 (1996)
[16] Bay, H., Tuytelaars, T., Van Gool, L.: SURF: Speeded Up Robust Features. In: Leonardis, A., Bischof, H., Pinz, A. (eds.) ECCV 2006, Part I. LNCS, vol. 3951, pp. 404–417. Springer, Heidelberg (2006)
[17] Lowe, D.G.: Distinctive Image Features from Scale-Invariant Keypoints. Int. J. Comput. Vis. 60(2), 91–110 (2004)
[18] Harris, C., Stephens, M.: A combined corner and edge detector. In: Proc. of Fourth Alvey Vision Conference, pp. 147–151 (1988)
[19] Lv, Q., Josephson, W., Wang, Z., Charikar, M., Li, K.: Multi-probe LSH: Efficient Indexing for High-dimensional Similarity Search. In: Proceedings of the 33rd International Conference on Very Large Data Bases, Vienna, Austria, pp. 950–961 (2007)

[20] Cayton, L.: Algorithm for manifold learning. University of California, CS2008-0923 (2006)
[21] Satopaa, V., Albrecht, J., Irwin, D., Raghavan, B.: Finding a 'Kneedle' in a Haystack: Detecting Knee Points in System Behavior. In: 31st ICDCSW, 166–171 (2011)
[22] Ioannides, M., Hadjiprocopi, A., Doulamis, N., Doulamis, A., Protopapadakis, E., Makantasis, K., Santos, P., Fellner, D., Stork, A., Balet, O., Julien, M., Weinlinger, G., Johnson, P.S., Klein, M., Fritsch, D.: Online 4D Reconstruction Using Multi-images Available Under Open Access. ISPRS Ann. Photogramm. Remote Sens. Spat. Inf. Sci. II-5/W1, 169–174 (2013)